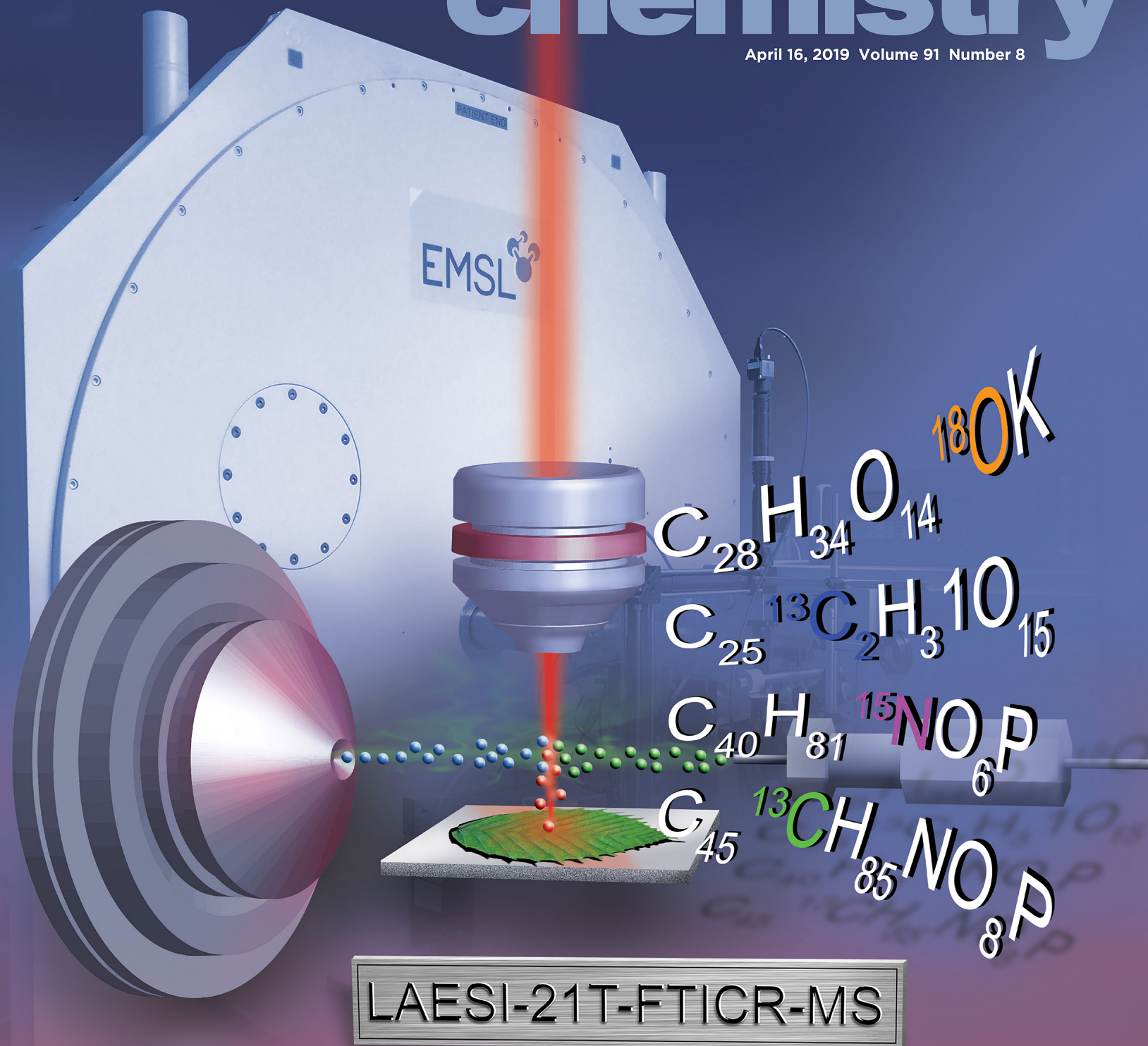


analytical chemistry

April 16, 2019 Volume 91 Number 8



ACS Publications
Most Trusted. Most Cited. Most Read.

www.acs.org

Ambient Metabolic Profiling and Imaging of Biological Samples with Ultrahigh Molecular Resolution Using Laser Ablation Electrospray Ionization 21 Tesla FTICR Mass Spectrometry

Sylwia A. Stopka,[†] Laith Z. Samarah,[†] Jared B. Shaw,[‡] Andrey V. Liyu,[‡] Dušan Veličković,[‡] Beverly J. Agtuca,[§] Caroline Kukolj,[§] David W. Koppenaal,[‡] Gary Stacey,[§] Ljiljana Paša-Tolić,[‡] Christopher R. Anderton,^{*,‡} and Akos Vertes^{*,†}

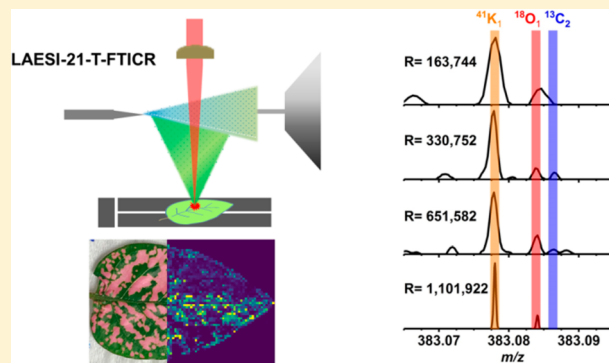
[†]Department of Chemistry, The George Washington University, Washington, D.C. 20052, United States

[‡]Environmental Molecular Sciences Laboratory and Biological Sciences Division, Pacific Northwest National Laboratory, Richland, Washington 99354, United States

[§]Divisions of Plant Sciences and Biochemistry, C. S. Bond Life Sciences Center, University of Missouri, Columbia, Missouri 65211, United States

Supporting Information

ABSTRACT: Mass spectrometry (MS) is an indispensable analytical tool to capture the array of metabolites within complex biological systems. However, conventional MS-based metabolomic workflows require extensive sample processing and separation resulting in limited throughput and potential alteration of the native molecular states in these systems. Ambient ionization methods, capable of sampling directly from tissues, circumvent some of these issues but require high-performance MS to resolve the molecular complexity within these samples. Here, we demonstrate a unique combination of laser ablation electrospray ionization (LAESI) coupled with a 21 tesla Fourier transform ion cyclotron resonance (21T-FTICR) for direct MS analysis and imaging applications. This analytical platform provides isotopic fine structure information directly from biological tissues, enabling the rapid assignment of molecular formulas and delivering a higher degree of confidence for molecular identification.



The ability to capture and visualize the complex metabolic composition of living organisms in situ is a bioanalytical grand challenge that has yet to be fully addressed. Due to their excellent sensitivity and selectivity, mass spectrometry (MS)-based platforms offer a unique opportunity to characterize an array of biomolecules.^{1,2}

Currently, the most common method for small molecule identification within biological samples is based on liquid chromatography (LC) separation followed by tandem MS measurements for structural information.^{3,4} However, this method requires extensive sample preparation, and the spatial information about the origin of a given molecule is often lost.⁵

Ambient ionization methods that require minimal to no sample preparation, like desorption electrospray ionization (DESI and nano-DESI) and laser ablation electrospray ionization (LAESI), demonstrated the ability to analyze and spatially map biomolecule distributions within live organisms.^{6–9} These direct sampling methods can provide molecular information, but a challenge presented by these ionization approaches is the complex mass spectral data they produce, due in part to the lack of a separation step. This can be partially overcome by introducing ion mobility separation (IMS-MS),

which can distinguish isobaric species, improve metabolite identification via collision cross section measurements, and increase overall molecular coverage and selectivity.^{10–13}

Alternative routes for improved confidence in biomolecular annotations also include coupling these ion sources with ultrahigh performance mass analysis instrumentation capable of resolving, identifying, and quantifying a full array of molecular species native to these systems. Specifically, the mass resolution attainable by Fourier transform ion cyclotron resonance (FTICR)-MS can minimize molecular interferences and increase the MS-peak capacity. FTICR-MS at high magnetic field strength can routinely deliver low parts-per-billion mass accuracy and a mass resolution (R) of $>1\,000\,000$.^{14,15} This level of performance facilitates more confident molecular annotation of cellular and extracellular components based on measuring the isotopic fine structure (IFS).^{16–19} However, even at this ultrahigh resolution,

Received: November 4, 2018

Accepted: March 1, 2019

Published: March 1, 2019

structural isomers cannot be resolved. All key measures of FTICR-MS performance improve with increased magnetic field strength (e.g., mass resolution, acquisition speed, dynamic range, etc.).²⁰ Recently, it has been demonstrated that the unique ultrahigh resolution 21 tesla (21T)-FTICR mass spectrometer at the Environmental Molecular Science Laboratory (EMSL) is capable of superior molecular specificity and sensitivity, characterized by spectral resolution above 10 million.^{14,21}

The capabilities of high-field FTICR-MS also confer unique advantages for MS imaging (MSI) by the ability to simultaneously determine the spatial distributions for hundreds of biomolecules, e.g., metabolites, lipids, peptides, and xenobiotics, within complex biological systems.^{22–24} Matrix-assisted laser desorption ionization (MALDI) and secondary ion mass spectrometry (SIMS) remain the most common MSI methods.^{25,26} However, the application of an exogenous matrix and the limited availability of commercial sources that operate under atmospheric pressure²⁷ have significantly prohibited the ability of MALDI to be useful for in situ biomolecular mapping of living systems. High vacuum requirements, extensive ion fragmentation, and moderate upper mass limit for the analyte also curtail the applicability of SIMS for in situ biological studies. There are a number of previously published examples of spatial probing sources exploiting the benefits of FTICR-MS,^{28,29} including infrared matrix-assisted laser desorption electrospray ionization (IR-MALDESI).³⁰

Herein, we demonstrate the utility of coupling a laser-based ambient ionization source, LAESI, to the 21T-FTICR mass spectrometer for the characterization of biomolecules directly from intact biological tissues and using IFS measurements for highly confident molecular formula annotations.

MATERIALS AND METHODS

Biological Samples. *Glycine max* (Williams 82) soybean seeds were sterilized with 20% (v/v) bleach solution followed by five water rinse cycles. A sterilized 3:1 vermiculite/perlite mixture was used as potting material for the seeds. The pots containing the seeds were placed in a greenhouse at a temperature of 30 °C and 16 h/8 h light/dark illumination cycle. At day 3, the plants were inoculated with 1 mL of *Bradyrhizobium japonicum* (USDA110 cells) suspension (10⁸ cells/mL) cultured in HM medium.³¹ Soybean root nodules were harvested at day 21. Whole root segments containing the nodules were cut and snap frozen in liquid nitrogen and then stored at –80 °C until the analysis. For LAESI-MS measurements, whole nodules were cut in half using a sterilized scalpel and placed onto a microscope slide. The slide was mounted on a Peltier stage set to –2 °C to minimize sample degradation.

Whole mouse kidneys were generously provided by Guanshi Zhang and Kumar Sharma (UT-Health San Antonio, TX, USA). Frozen kidneys were cut into 10 μm thick sections using a cryomicrotome (Cryostar NX70; Thermo Scientific, San Jose, CA, USA), thaw-mounted onto glass slides, and stored at –80 °C until analysis. For LAESI-MS measurements, the slides were mounted onto the Peltier stage set to –10 °C to minimize the degradation of the sample and maintain its water content.

Common coleus leaves were harvested from a live plant. *Mentha piperita* (peppermint) and *Hypoestes phyllostachya* (Polka dot) plants were obtained from a local gardening supply store. For all experiments, leaves were freshly harvested by

snipping the stem at the base of the leaf. They were attached to glass slides using double-sided tape, and the slides were mounted onto the Peltier stage set to 0 °C to minimize sample degradation.

LAESI-21T-FTICR Mass Spectrometer. A LAESI ion source was constructed on the basis of the design described in the literature⁷ and adapted to fit an LTQ Orbitrap Velos and the 21T-FTICR mass spectrometers (see schematic in Figure 1). A mid-IR laser source (IR Opolette HE 2940; Opotek,

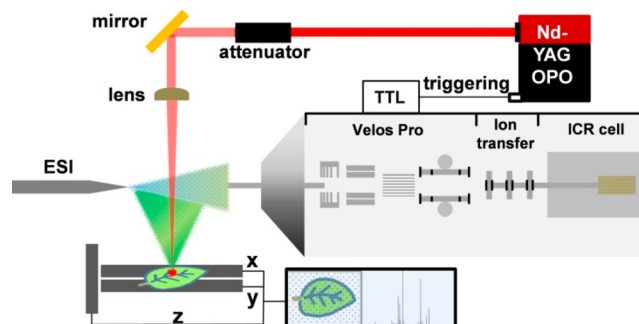


Figure 1. Schematic of the LAESI source coupled with 21T-FTICR-MS. Here, 2.94 μm wavelength laser pulses (20 Hz) are focused and delivered onto water-rich samples mounted on a custom-built Peltier stage motorized XYZ translation stage combination. The resulting ablation plume is intercepted by an ESI stream, delivering ionized material to be analyzed by 21T-FTICR-MS. This configuration also permitted generation of MS images for biological samples. Photos of the actual system can be seen in Figure S3.

Carlsbad, CA, USA) operating at a fixed 2.94 μm wavelength was used to deliver 7 ns laser pulses. They were attenuated to energies between 1 and 6 mJ/pulse with a shot-to-shot RSD of <5%. The laser beam was steered by gold-coated mirrors to a 50 mm focal length plano-convex CaF₂ focusing lens (LA5763; Thorlabs, Newton, NJ, USA) held by a 30 mm cage system. A Peltier stage mounted on a motorized XYZ translation stage (Zaber Technologies, Vancouver, BC, Canada) was used to adjust the temperature of the sample between –10 and 0 °C. For all measurements, the relative humidity in the laboratory was <15%, which prevented the formation of condensation on the tissues during analysis.

As the mass spectrometer inlet orifice temperature was set to 325 °C, a 25.4 mm long inlet capillary was used to reduce sample surface heating, accommodate the LAESI optics, and permit extended stage movement. A stainless steel ESI emitter (MT320-50-5-5; New Objective, Woburn, MA, USA) was placed on-axis with the extended inlet capillary at a distance of 10 to 12 mm. In positive ion mode, an ESI solution of 1:1 MeOH/water (v/v) with 0.1% acetic acid was sprayed with an emitter voltage of +3.3 kV, whereas for negative ion mode, a solution of 2:1 of MeOH/CHCl₃ (v/v) was used with an emitter voltage of –2.5 kV. In both cases, the spray solution flow rate was set to 500 nL/min. The laser pulses impinging on the sample produced an ablation plume, consisting mostly of neutrals that expanded into the electrospray resulting in ion formation. The produced ions were sampled by either the LTQ Orbitrap Velos or the 21T-FTICR mass spectrometer.

The instrumental setup and conditions for the 21T-FTICR mass spectrometer were as detailed elsewhere.¹⁴ Mass calibration for both instruments was periodically performed using Pierce LTQ ESI positive and negative ion calibration

solutions (Thermo Fisher Scientific, Waltham, MA, USA). Time-domain signal processing, including apodization and zero filling, as well as external mass calibration were performed by the onboard FT acquisition computer. Magnitude mode mass spectra were stored in reduced profile mode in the .RAW file format. We utilized the tools in Xcalibur for peak picking in profile mode.

Triggering of the laser and stage movement were synchronized with the mass spectrometer using a data acquisition board (NI USB-6341; National Instruments, Austin, TX, USA) and a custom-developed LabVIEW program. A TTL pulse was sent from the front-end ion trap when it was ready to accumulate ions. This pulse initiated a trigger to fire the flashlamp of the laser followed by a second trigger, with a controllable delay time, to open the Q-switch and deliver a laser pulse to the sample. This synchronization maximized the collection of sample-related ions, as the laser only fired when the mass spectrometer was ready to collect ions. As at 20 Hz repetition rate, the time between laser shots was 50 ms, and ion trap fill times were varied between 50 and 200 ms to permit one to four laser pulses per filling event, respectively.

For spatial probing applications (e.g., imaging), the Peltier stage was mounted on the high-resolution motorized XYZ translation stage. The custom-designed LabVIEW software allowed the operator to move the stage remotely or move automatically during an imaging experiment. For the latter, the trigger was received from the mass spectrometer; the laser was fired, and the stage was moved to its next predetermined position. The program only allowed the laser to fire after the following MS trigger if the stage had reached the next position. For the imaging experiments, both MS instruments were set to collect ions for 200 ms with the automatic gain control (AGC) turned off, and four laser pulses (~1.6 mJ) were delivered to the sample at each pixel location. The AGC was turned off to capture all the ions that are generated from our laser pulses.

Data Analysis. Data acquisition files consisted of initial spectra that contained only blank ESI signal, followed by sample-related spectra. Processing of mass spectra was performed using the Xcalibur software (3.0.63; Thermo Fisher Scientific Inc., Bremen, Germany). Here, the ESI only spectra were background subtracted from the sample-related spectra in an effort to identify sample-related species. For selected precursor ions, mass defects were calculated to identify isotopologues. In general, gains of 0.9970, 1.0034, 1.0042, 1.9971, 1.9981, 2.0042, and 2.0068 Da from the precursor ion were associated with the presence of natural isotopes $^{15}\text{N}_1$, $^{13}\text{C}_1$, $^{17}\text{O}_1$, $^{37}\text{Cl}_1$, $^{41}\text{K}_1$, $^{18}\text{O}_1$, and $^{13}\text{C}_2$. The presence and relative abundances of these isotopes in the IFS are only consistent with a few chemical formulas. Note that many of the available software packages to derive an elemental formula from IFS spectral features were developed for petroleomics and other complex organic mixtures and were not ideally suited for our analysis. For example, compounds in complex biological samples can be detected as a range of adducts (e.g., $[\text{M} + \text{K}^+]$ and $[\text{M} + \text{Na}^+]$), which are not recognized by these software platforms. Given that we only have a few hundred spectral features, we performed annotations manually. The accurate mass of the precursor ion and knowledge of specific elements present on the basis of the measured IFS were used to obtain potential chemical formulas with <1 ppm accuracy by using the web-based ChemCalc software (http://www.chemcalc.org/mf_finder). Once the potential formulas were obtained, manual comparison of theoretical and experimental relative

abundances of the isotopes was performed by the enviPat Web 2.2 software (<https://www.envipat.eawag.ch/index.php>) with the resolution parameter set to that of the experimental value for the precursor. To show the agreement between the theoretical and measured abundances as a function of transient time (TT), we included Figure S6 depicting the IFS of a disaccharide at $M + 2$ for TT = 0.768, 1.536, and 3.072 s. For all of these TT values, the theoretical and measured relative intensities were comparable.

Additionally, the R package IsoSpec¹³ was used to obtain the theoretical m/z values for the isotopologues based on their potential chemical formulas and provided the elemental composition for each mass. Following these selection steps, a single chemical formula was selected (see Table S1–S4). Putative compound annotations were made by matching accurate mass data (0.4 ppm threshold) in the METLIN database, unless otherwise noted (see Figure S1). We observed a uniform distribution of errors across all masses in the m/z 200–900 range (see Figure S1a). Likewise, the mass error was independent of the peak intensities in this data set (see Figure S1b).

Imaging data was acquired by serially capturing mass spectra over a given number of scans, where the number of scans was determined by the number of pixels in the image being captured (1 spectrum per pixel). For all images, a 300 μm step size was used between pixels (focal spot size for the laser beam was ~200 μm). The resulting Thermo RAW data files were then converted to imzML format using imzMLconverter 2.0 (generously provided by Alan Race). The imzML files and accompanying ibd files (image indexing files) were both uploaded to METASPACE (<http://metaspace2020.eu>) and processed using SCiLS lab (Bruker Daltonics, Billerica, MA, USA). Tentative molecular identifications were made using both the SwissLipids and HMDB v2.5-Cotton databases in METASPACE. Visualization of the mass spectral imaging and ion image data was performed using SCiLS. Ion images were normalized to the total ion current, and hot spot removal was performed. For the Common coelus images in Figure S2, weak denoising was used for visualizing the imaging data. These images were registered to the optical images of the leaf tissue prior to LAESI-MS analysis. High-resolution images of the ablated plant tissue, which demonstrate the laser spot size, were acquired using an optical microscope. The link to the METASPACE data for Figure S2 is noted in the figure caption below, and the data for Figure 4 can be found here: http://metaspace2020.eu/#/annotations?ds=2018-02-25_03h57m39s&sort=-mz§ions=1.

RESULTS AND DISCUSSION

Instrumental Design and Figures of Merit. Development and optimization of the LAESI source with the custom software and motorized stage was performed on a Velos LTQ Orbitrap mass spectrometer (Figure S3a,b). Then, the optimized LAESI source⁹ was coupled to the 21T-FTICR mass spectrometer (Figures 1 and S3c,d).¹⁴ As noted elsewhere,^{30,32,33} we observed a pronounced decrease in signal variability when laser triggering was synchronized with ion trap timing (Figure S4). The limit of detection (LOD) for multiple molecules was compared with the LAESI source coupled to the Orbitrap system and the 21T-FTICR mass spectrometer, using the same transient times (TT = 1.05 s) for both instruments. In positive ion mode, the LOD of verapamil was determined to be 10 fmol for both FTMS platforms and was comparable to

the LOD of 8 fmol determined previously for a LAESI source coupled to a time-of-flight (TOF) mass spectrometer.⁷

The negative ion mode sensitivity for sucrose was lower, with an LOD of 1 pmol for both systems (Figure S5). It is worth noting that while the sensitivity of both FTMS-based systems was comparable, using the same TT, the 21T-FTICR mass spectrometer had nearly a 3-fold increase in measured mass resolution over the Orbitrap system ($R = \sim 325\,000$ vs $118\,000$ at m/z 455.29). This increased mass resolution also exhibited a benefit when utilizing this source for MSI (Figure S2). Specifically, in imaging freshly harvested common coleus leaves, we observed an increase in the number of molecular annotations, from 8 to 106, in METASPACE using the SwissLipids database with a 20% false discovery rate (FDR).³⁴

Instrumental Design and Figures of Merit. To further improve the mass resolution of the 21T-FTICR mass spectrometer, the TT can be increased and/or absorption mode can be implemented.¹⁴ By doing the former, we were able to obtain IFS information for a number of species directly from soybean nodule samples (Tables S1 and S2), freshly harvested mint leaves (Table S3), and mouse kidney sections (Table S4). A trade-off was observed between sensitivity and mass resolution; thus, to obtain IFS measurements, the TT was adjusted to obtain the optimum R for apodized time domain signal, in which IFS spectral features were resolved (Figure 2). From previous LAESI-TOF-MS analysis of root nodules, we selected spectral features that pertained to [disaccharide + K]⁺ and [heme b]⁺ to demonstrate the IFS capabilities.⁹ Note that, to obtain IFS features of a sample related ion, the optimum TT

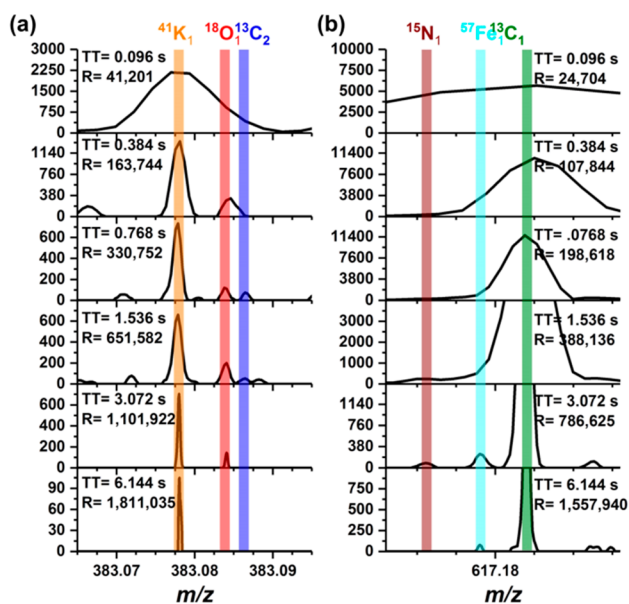


Figure 2. Optimizing mass resolution required to deconvolute IFS features in spectra from a 100 μm thick soybean root nodule section using LAESI-21T-FTICR. Transient time (TT) was varied from 0.096 to 6.144 s ($R_{\text{max}} = \sim 40\,000$ to $2\,000\,000$, for apodized time domain signal, respectively). (a) Determining the optimum TT = 0.768 s and corresponding mass resolution, $R = 330\,752$, to resolve the IFS for the $M + 2$ peak of the monoisotopic disaccharide peak (m/z 381.0799, K^+ -adduct), where the $^{41}\text{K}_1$ (orange), $^{18}\text{O}_1$ (red), and $^{13}\text{C}_2$ (blue) spectral locations were annotated. (b) Determining the optimum TT = 3.072 s and $R = 786\,625$ to resolve the IFS for the $M + 1$ peak of the monoisotopic heme b peak (m/z 616.1778), where the $^{15}\text{N}_1$ (dark red), $^{57}\text{Fe}_1$ (teal), and $^{13}\text{C}_1$ (green) spectral locations were annotated.

was dependent on the size of the molecule (i.e., the m/z value).³⁵ In the example of a smaller molecule at a nominal mass of 381, all three $M + 2$ isotopologues of the disaccharide (Figure 2a) were resolved (e.g., $^{41}\text{K}_1$, $^{16}\text{O}_1$, and $^{13}\text{C}_2$) with a TT = 0.75 s that corresponded to a measured $R = 330\,752$. At this TT, the theoretical and relative natural isotope abundances matched well. For the larger heme b molecule with a nominal mass of 616, a TT = 6 s (measured $R = 786\,685$) was required to resolve the $^{15}\text{N}_1$, $^{57}\text{Fe}_1$, and $^{13}\text{C}_1$ $M + 1$ IFS spectral features. As noted, a limitation to increasing the TT is the decrease in analytical sensitivity due to signal decay.¹⁴

The IFSs of an additional 77 ions were measured directly for different tissue types using the LAESI-21T-FTICR mass spectrometer (Tables S1–S4). For example, the putatively annotated flavonoids, with molecular formulas of $\text{C}_{27}\text{H}_{31}\text{O}_{15}$ and $\text{C}_{28}\text{H}_{34}\text{O}_{15}$, were measured directly from a mint leaf (Figure 3a). Putatively annotated lipids, with molecular formulas of $\text{C}_{40}\text{H}_{81}\text{NO}_6\text{P}$ and $\text{C}_{46}\text{H}_{85}\text{NO}_8\text{P}$, were measured from a 10 μm thick mouse kidney tissue section (Figure 3b) at a TT of 3.072 s. For the 300 most abundant peaks in a typical soybean root nodule LAESI mass spectrum, the trade-off resolutions at varied TT values were presented in Figure S7. The optimal TT values were manually selected for each ion that was annotated.

Lastly, we were able to attain the same IFS spectral information on disaccharide and heme b, shown in Figure 2, directly from a soybean root nodule that was cut in half prior to placing it on the sample stage (Figure 3c). Additional IFS isotopologues were ascertained in negative ion mode directly from these soybean root nodules (Figure S8). Furthermore, detecting unique metal isotopologue IFS features (e.g., $\text{C}_{34}\text{H}_{32}\text{N}_4\text{O}_4\text{Fe}$ and $\text{C}_{55}\text{H}_{73}\text{N}_4\text{O}_5\text{Mg}$) provides more confidence in the organometallic molecular identification of heme b and chlorophyll a, respectively.

A total of 77 compounds were annotated using IFS spectral information directly from biological tissues. The mass error values were <0.4 ppm for all identifications. This relatively large error cutoff can be attributed to the varying number of ions in the cell (i.e., AGC is off), together with the use of external calibration.

These results illustrated the potential of LAESI-21T-FTICR-MS for directly obtaining high confidence chemical formula annotations of molecules based on IFS spectral fingerprints. However, without a separation step, even at this ultrahigh mass resolution, structural isomers are not resolved. For example, in soybean root nodules, m/z 293.0211 corresponded to $\text{C}_{15}\text{H}_{10}\text{O}_4\text{K}$ with a -0.05 ppm error based on IFS measurements. Using the Metlin database, there were 22 potential hits for dihydroxyflavone and its structural isomers with an identical chemical formula. This was also true for other detected compounds in Tables S1–S4. Along with other analytical approaches, and following the guidelines of the Metabolomics Standards Initiative,³⁶ IFS can improve metabolite identification and provide insight for molecular compositions and distributions within complex biological systems.

Ultrahigh Mass Resolution MS Imaging. We demonstrated the utility of high mass resolution for IFS molecular mapping directly from a freshly harvested Polka dot plant leaf (*Hypoestes phyllostachya*). The 5307-pixel imaging experiment was conducted using a TT of 6.144 s, and on the basis of the sum of the required dwell time and stage repositioning time, it took ~ 9.6 h to capture. During this time, the mass accuracy of

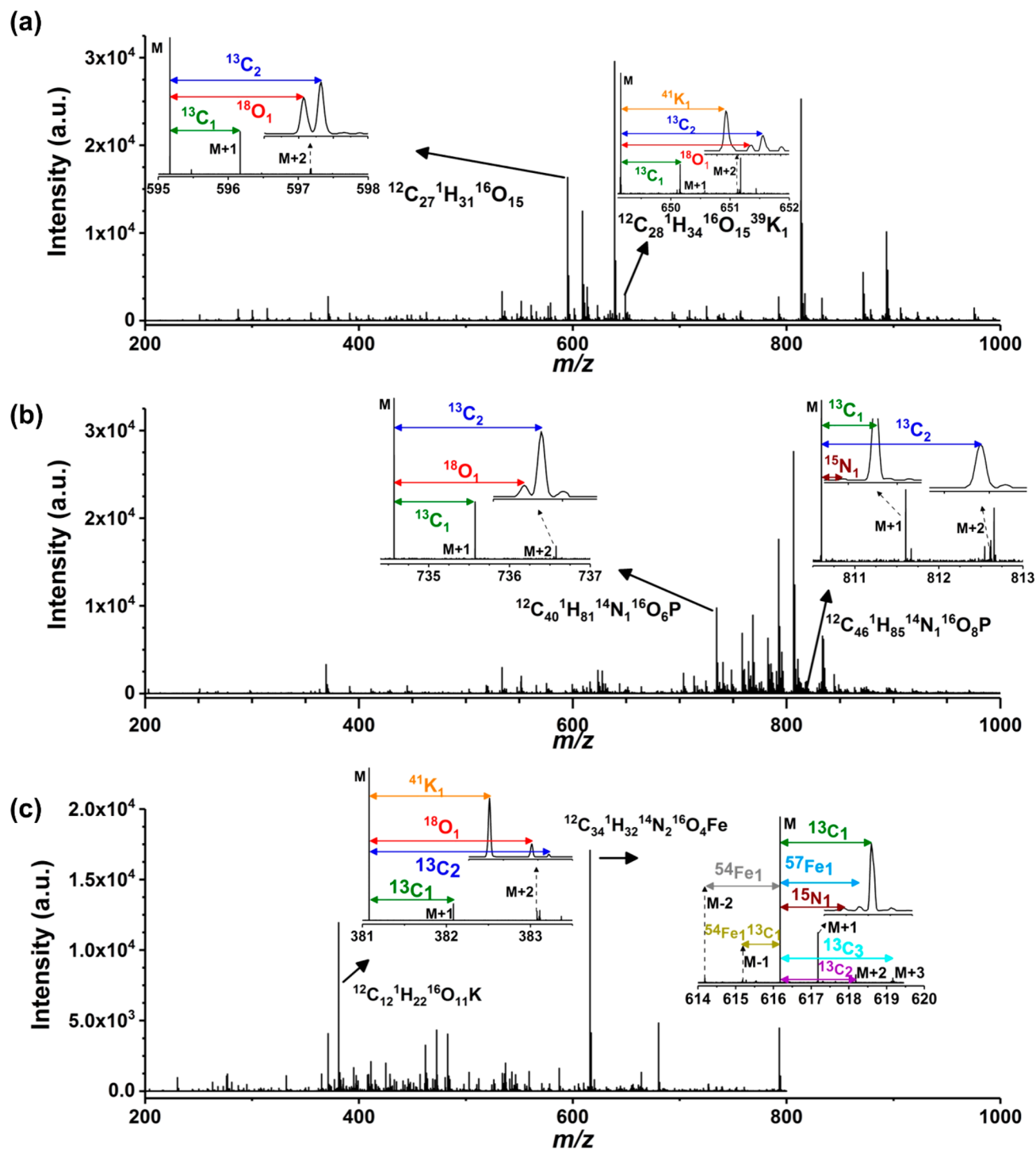


Figure 3. Molecular formulas of species determined directly from different tissue types based upon IFS spectra. Here, the LAESI mass spectra were acquired from (a) freshly harvested mint leaf, (b) a 10 μm mouse kidney section, and (c) a soybean root nodule cut in half. (a) Molecular formulas for two tentatively identified flavonoids, $\text{C}_{27}\text{H}_{31}\text{O}_{15}$ and $\text{C}_{28}\text{H}_{34}\text{O}_{15}\text{K}$, were characterized from a mint leaf. (b) Molecular formulas $\text{C}_{40}\text{H}_{81}\text{NO}_6\text{P}$ and $\text{C}_{46}\text{H}_{85}\text{NO}_8\text{P}$, putatively identified as lipids, were determined from mouse kidney. (c) IFS spectral features revealed monoisotopic species at m/z 381.0799 and 616.1778 from soybean root nodules as $\text{C}_{12}\text{H}_{22}\text{O}_{11}$ and $\text{C}_{34}\text{H}_{32}\text{N}_2\text{O}_4\text{Fe}$, respectively. More comprehensive lists of molecular formulas annotated from these spectra are in Tables S1–S4. Soybean root nodule was studied in both positive and negative ion mode. In the other two examples, LAESI-MS was performed in positive ion mode.

the monoisotopic peak for chlorophyll a varied 0.89 ppm. This was the consequence of the highly variable number of ions in the cell caused by shot-to-shot variations in ion generation. The shot-to-shot variations in S/N across the image are mostly attributed to various “matrix effects”, including differences in localized salt concentrations and charge competition between

analytes. We observed that the ion image of the monoisotopic peak of chlorophyll a (Figure 4b, $\text{C}_{55}\text{H}_{73}\text{Mg}_{14}\text{N}_4\text{O}_5$) correlated well with the optical image of the green leaf tissue pigments (Figure 4a, inset). Within the average spectrum across the tissue, multiple isotopic species were resolved around each of the corresponding $M + 1$, $M + 2$, and $M + 3$ peaks from the

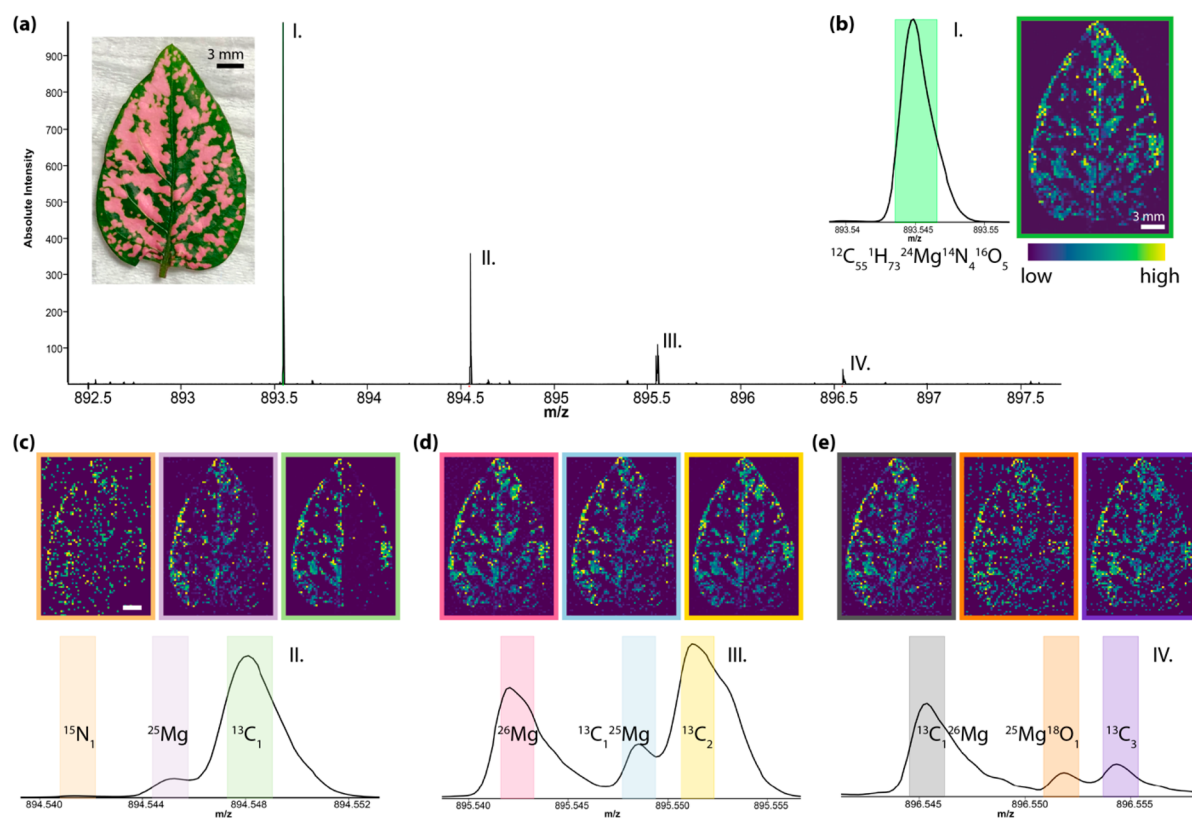


Figure 4. Visualizing IFS of chlorophyll a (chl a) from a *H. phyllostachya* leaf by MSI using LAESI-21T-FTICR-MS. (a) Average spectrum obtained over the entire leaf area (image inset) in the m/z 892.5 to 897.5 range, where $R = \sim 1\,111\,000$ at m/z 893.5 was attained at each pixel. (b) Selection of the monoisotopic peak (I) illustrates the distribution of chlorophyll a across the leaf tissue, which correlates well with the optical image of the green tissue area of the leaf. (c–e) The spectra and corresponding ion images related to the isotopic peaks at $M + 1$, $M + 2$, $M + 3$ Da (II–IV) from the monoisotopic peak, respectively. Data was acquired in positive ion mode for 5307 pixels with a TT of 6.144 s. For all images, peaks were selected with a ± 0.190 mDa window. This data can be visualized in METASPACE (see link for the images in the [Supporting Information](#)), where it is annotated with a 5% FDR by fitting the monoisotopic, $^{13}\text{C}_1$, ^{26}Mg , and $^{13}\text{C}_2$ peaks and correlating their respective ion images.

precursor ion (Figure 4c–e, respectively). The ion images of each of these isotopologues compared well with the ion image of the monoisotopic peak and the optical image of the green pigment in the leaf indicating that they likely correspond to the same molecular species. Even with the ultrahigh mass resolution of 21T-FTICR-MS, selected so the TT is still practical for imaging, many species remained unresolved and contributed to some of the annotated peaks. For example, the $^{18}\text{O}_1$ peak is one of five much less abundant species unresolved from what is annotated as the $^{13}\text{C}_1^{25}\text{Mg}$ peak in Figure 4d. Multiple unresolved isotopic species contribute to the $^{13}\text{C}_1$, ^{26}Mg , $^{13}\text{C}_2$, $^{13}\text{C}_2^{25}\text{Mg}$, $^{13}\text{C}_2$, $^{13}\text{C}_2^{26}\text{Mg}$, $^{25}\text{Mg}^{18}\text{O}_1$, and $^{13}\text{C}_2$ annotated peaks, but these species are the most naturally abundant at their respective masses. Comparing the ion images of the different isotopic peaks, as METASPACE does by a spatial isotope measurement,³⁴ also increases confidence in molecular annotations. As such, a 5% FDR was determined for the molecular formula $^{12}\text{C}_{55}^{1}\text{H}_{73}^{24}\text{Mg}^{14}\text{N}_4^{16}\text{O}_5$ of this species using METASPACE. In all, 195 molecular formula annotations were generated from the LAESI-21T-FTICR-MS data acquired on the *H. phyllostachya* leaf (see METASPACE link in the [Materials and Methods](#) for the annotations), with a 20% FDR using the Human Metabolome Database (HMDB)-Cotton database.

CONCLUSIONS

In conclusion, we demonstrated the benefit of coupling an ambient ionization technique, LAESI, to the 21T-FTICR mass spectrometer for the characterization of biomolecules directly from a number of different biological tissues. The performance of this instrument was highlighted in comparison to a less powerful FT-based MS that was used to develop the LAESI source. We observed comparable analytical sensitivity for the two systems, with increased mass resolution using the 21T-FTICR-MS. We further showed that obtaining IFS features from intact biological samples required fine adjustments of the TT for the m/z range being analyzed. Throughout this study, we were aiming to find a trade-off between sensitivity and ultimate spectral resolution to maximize usable IFS information.

In all the examples shown here, having the IFS spectral information helped one make more confident chemical formula annotations that could translate to metabolite identifications. In the cases of the plant tissues analyzed, we demonstrated the speed and ease with which we could obtain direct metabolic information from these tissues, as we could take freshly harvested tissues and probe them directly. These advantages were further expounded in the MSI of leaf tissues, where correlating ion images of the isotopic peaks with optical images of variegation patterns improved confidence in molecular formula annotations. Finally, the development of this unique ultrahigh resolution ambient MS instrument

further narrows the gap in the creation of analytical instrumentation capable of imaging, identifying, and quantifying a full array of native molecules within complex living biological systems. In future LAESI experiments, we plan to utilize a software developed at PNNL, Formularity,¹⁹ that will permit automated elemental annotations based on IFS features, as well as capture and characterize potential adducts that are more ubiquitous in the MS analysis of biological samples. The LAESI 21T-FTICR-MS capability is located within the EMSL User Facility and is available to researchers worldwide.

■ ASSOCIATED CONTENT

■ Supporting Information

The Supporting Information is available free of charge on the ACS Publications website at DOI: [10.1021/acs.analchem.8b05084](https://doi.org/10.1021/acs.analchem.8b05084).

Mass measurement errors as a function of m/z and peak intensities; comparison of LAESI-MS images with LTQ Orbitrap Velos and 21T-FTICR; images of home-built LAESI source; LAESI-MS peak intensities for verapamil solutions of different concentrations; sensitivities for LAESI-MS with LTQ Orbitrap Velos and 21T-FTICR mass spectrometers; comparison of LAESI mass spectra for soybean root nodule at three different TT; resolving power for 300 peaks with the highest absolute intensities; isotopic fine structure acquired directly from a root nodule using LAESI-MS (PDF)

Annotations for IFS peaks of LAESI-21T-FTICR spectra of nodules, leaves, and mouse kidneys (XLSX)

■ AUTHOR INFORMATION

Corresponding Authors

*E-mail: vertes@gwu.edu. Phone: +1 (202) 994-2717. Fax: +1 (202) 994-5873.

*E-mail: christopher.anderton@pnnl.gov. Phone: +1 (509) 371-7970. Fax: +1 (509) 371-7866.

ORCID

Sylwia A. Stopka: [0000-0003-3761-6899](https://orcid.org/0000-0003-3761-6899)

Jared B. Shaw: [0000-0002-1130-1728](https://orcid.org/0000-0002-1130-1728)

Christopher R. Anderton: [0000-0002-6170-1033](https://orcid.org/0000-0002-6170-1033)

Akos Vertes: [0000-0001-5186-5352](https://orcid.org/0000-0001-5186-5352)

Author Contributions

A.V., G.S., L. P.-T., D.W.K., and C.R.A. conceived the research. S.A.S., L.Z.S., C.K., D.V., and C.R.A. performed the experiments. B.J.A. and J.B.S. assisted in the instrumental configuration of the LAESI source with the custom 21T-FTICR MS. B.J.A. grew the soybean plants and provided the nodules for analysis. A.V.L. developed and provided programing software for the automated sample stage. S.A.S., C.R.A., and A.V. performed the data analysis and wrote the manuscript with input from G.S., L.P.-T., and D.W.K.

Notes

The authors declare no competing financial interest.

■ ACKNOWLEDGMENTS

This material is based work supported by the U.S. Department of Energy, Office of Biological and Environmental Research under award number DE-SC0013978. Additional support was provided by University of Missouri's Gus T. Ridgel Fellowship and George Washington Carver Fellowship (B.J.A.) as well as grant no. IoS-1734145 from the National Science Foundation

Plant Genome Program (to G.S.). We would like to thank Yaya Cui for his help with growing and inoculating numerous soybean plants and Guanshi Zhang and Kumar Sharma at UT-Health San Antonio for providing the kidney tissue. The design parameters and component list for the Peltier stage were kindly provided by Jarod A. Fincher of GWU. We also thank Alan Race for his assistance in converting imaging data to imzML files and Dirk Hoelscher (MPI Jena) for generating the HMDB-Cotton related list of molecules (METASPACE).

■ REFERENCES

- (1) Dettmer, K.; Aronov, P. A.; Hammock, B. D. *Mass Spectrom. Rev.* **2007**, *26*, 51–78.
- (2) Jorge, T. F.; Rodrigues, J. A.; Caldana, C.; Schmidt, R.; van Dongen, J. T.; Thomas-Oates, J.; Antonio, C. *Mass Spectrom. Rev.* **2016**, *35*, 620–649.
- (3) Zhou, B.; Xiao, J. F.; Tuli, L.; Resson, H. W. *Mol. BioSyst.* **2012**, *8*, 470–481.
- (4) Hufsky, F.; Böcker, S. *Mass Spectrom. Rev.* **2017**, *36*, 624–633.
- (5) Xiao, J. F.; Zhou, B.; Resson, H. W. *TrAC, Trends Anal. Chem.* **2012**, *32*, 1–14.
- (6) Takats, Z.; Wiseman, J. M.; Gologan, B.; Cooks, R. G. *Science* **2004**, *306*, 471–473.
- (7) Nemes, P.; Vertes, A. *Anal. Chem.* **2007**, *79*, 8098–8106.
- (8) Nguyen, S. N.; Liyu, A. V.; Chu, R. K.; Anderton, C. R.; Laskin, J. *Anal. Chem.* **2017**, *89*, 1131–1137.
- (9) Stopka, S. A.; Agtuca, B. J.; Koppelaar, D. W.; Paša-Tolić, L.; Stacey, G.; Vertes, A.; Anderton, C. R. *Plant J.* **2017**, *91*, 340–354.
- (10) Sans, M.; Feider, C. L.; Eberlin, L. S. *Curr. Opin. Chem. Biol.* **2018**, *42*, 138–146.
- (11) Shrestha, B.; Vertes, A. *Anal. Chem.* **2014**, *86*, 4308–4315.
- (12) Castro-Perez, J.; Roddy, T. P.; Nibbering, N. M. M.; Shah, V.; McLaren, D. G.; Previs, S.; Attygalle, A. B.; Herath, K.; Chen, Z.; Wang, S. P.; Mitnaul, L.; Hubbard, B. K.; Vreeken, R. J.; Johns, D. G.; Hankemeier, T. J. *Am. Soc. Mass Spectrom.* **2011**, *22*, 1552–1567.
- (13) Li, H.; Smith, B. K.; Mark, L.; Nemes, P.; Nazarian, J.; Vertes, A. *Int. J. Mass Spectrom.* **2015**, *377*, 681–689.
- (14) Shaw, J. B.; Lin, T.-Y.; Leach, F. E.; Tolmachev, A. V.; Tolić, N.; Robinson, E. W.; Koppelaar, D. W.; Paša-Tolić, L. *J. Am. Soc. Mass Spectrom.* **2016**, *27*, 1929–1936.
- (15) Hendrickson, C. L.; Quinn, J. P.; Kaiser, N. K.; Smith, D. F.; Blakney, G. T.; Chen, T.; Marshall, A. G.; Weisbrod, C. R.; Beu, S. C. *J. Am. Soc. Mass Spectrom.* **2015**, *26*, 1626–1632.
- (16) Miladinović, S. M.; Kozhinov, A. N.; Gorshkov, M. V.; Tsybin, Y. O. *Anal. Chem.* **2012**, *84*, 4042–4051.
- (17) Nagao, T.; Yukihira, D.; Fujimura, Y.; Saito, K.; Takahashi, K.; Miura, D.; Wariishi, H. *Anal. Chim. Acta* **2014**, *813*, 70–76.
- (18) Krajewski, L. C.; Rodgers, R. P.; Marshall, A. G. *Anal. Chem.* **2017**, *89*, 11318–11324.
- (19) Tolic, N.; Liu, Y.; Liyu, A.; Shen, Y. F.; Tfaily, M. M.; Kujawinski, E. B.; Longnecker, K.; Kuo, L. J.; Robinson, E. W.; Pasa-Tolic, L.; Hess, N. J. *Anal. Chem.* **2017**, *89*, 12659–12665.
- (20) Marshall, A. G.; Guan, S. *Rapid Commun. Mass Spectrom.* **1996**, *10*, 1819–1823.
- (21) Walker, L. R.; Tfaily, M. M.; Shaw, J. B.; Hess, N. J.; Pasa-Tolic, L.; Koppelaar, D. W. *Metallomics* **2017**, *9*, 82–92.
- (22) Klitzing, H. A.; Weber, P. K.; Kraft, M. L. *Methods Mol. Biol.* **2013**, *950*, 483–501.
- (23) Gemperline, E.; Keller, C.; Li, L. *Anal. Chem.* **2016**, *88*, 3422–3434.
- (24) Wu, C.; Dill, A. L.; Eberlin, L. S.; Cooks, R. G.; Ifa, D. R. *Mass Spectrom. Rev.* **2013**, *32*, 218–243.
- (25) Cornett, D. S.; Reyzer, M. L.; Chaurand, P.; Caprioli, R. M. *Nat. Methods* **2007**, *4*, 828–833.
- (26) Palmer, A.; Trede, D.; Alexandrov, T. *Metabolomics* **2016**, *12*, 107.
- (27) Römpf, A.; Guenther, S.; Takats, Z.; Spengler, B. *Anal. Bioanal. Chem.* **2011**, *401*, 65–73.

(28) Spraggins, J. M.; Rizzo, D. G.; Moore, J. L.; Rose, K. L.; Hammer, N. D.; Skaar, E. P.; Caprioli, R. M. *J. Am. Soc. Mass Spectrom.* **2015**, *26*, 974–985.

(29) Veličković, D.; Chu, R. K.; Carrell, A. A.; Thomas, M.; Pašatolić, L.; Weston, D. J.; Anderton, C. R. *Anal. Chem.* **2018**, *90*, 702–707.

(30) Robichaud, G.; Barry, J. A.; Garrard, K. P.; Muddiman, D. C. *J. Am. Soc. Mass Spectrom.* **2013**, *24*, 92–100.

(31) Cole, M. A.; Elkan, G. H. *Antimicrob. Agents Chemother.* **1973**, *4*, 248–253.

(32) Galicia, M. C.; Vertes, A.; Callahan, J. H. *Anal. Chem.* **2002**, *74*, 1891–1895.

(33) Rosen, E. P.; Bokhart, M. T.; Nazari, M.; Muddiman, D. C. *Anal. Chem.* **2015**, *87*, 10483–10490.

(34) Palmer, A.; Phapale, P.; Chernyavsky, I.; Lavigne, R.; Fay, D.; Tarasov, A.; Kovalev, V.; Fuchser, J.; Nikolenko, S.; Pineau, C.; Becker, M.; Alexandrov, T. *Nat. Methods* **2017**, *14*, 57.

(35) Makarov, A.; Denisov, E. *J. Am. Soc. Mass Spectrom.* **2009**, *20*, 1486–1495.

(36) Sumner, L. W.; Amberg, A.; Barrett, D.; Beale, M. H.; Beger, R.; Daykin, C. A.; Fan, T. W. M.; Fiehn, O.; Goodacre, R.; Griffin, J. L.; Hankemeier, T.; Hardy, N.; Harnly, J.; Higashi, R.; Kopka, J.; Lane, A. N.; Lindon, J. C.; Marriott, P.; Nicholls, A. W.; Reily, M. D.; Thaden, J. J.; Viant, M. R. *Metabolomics* **2007**, *3*, 211–221.

Supporting Information

Ambient Metabolic Profiling and Imaging of Biological Samples with Ultrahigh Molecular Resolution using Laser Ablation Electrospray Ionization 21 Tesla FTICR Mass Spectrometry

Sylwia A. Stopka,^a Laith Z. Samarah,^a Jared B. Shaw,^b Andrey V. Liyu,^b Dušan Veličković,^b
Beverly J. Agtuca,^c Caroline Kukulj,^c David W. Koppenaal,^b Gary Stacey,^c
Ljiljana Paša-Tolić,^b Christopher R. Anderton*^b and Akos Vertes*^a

^aDepartment of Chemistry, The George Washington University, Washington, DC 20052

^bEnvironmental Molecular Sciences Laboratory and Biological Sciences Division, Pacific Northwest National Laboratory, Richland, WA 99354

^cDivisions of Plant Sciences and Biochemistry, C. S. Bond Life Sciences Center, University of Missouri, Columbia, MO 65211

Table of Contents

| | |
|---|---|
| SUPPORTING FIGURES | 2 |
| Figure S1. Mass measurement errors as a function of m/z and peak intensities | 2 |
| Figure S2. Comparison of LAESI-MS images with LTQ Orbitrap Velos and 21T-FTICR | 3 |
| Figure S3. Images of homebuilt LAESI source | 4 |
| Figure S4. LAESI-MS peak intensities for verapamil solutions of different concentrations | 5 |
| Figure S5. Sensitivities for LAESI-MS with LTQ Orbitrap Velos and 21T-FTICR mass spectrometers | 6 |
| Figure S6. Comparison of LAESI mass spectra for soybean root nodule at three different TT 7 | 7 |
| Figure S7. Resolving power for 300 peaks with highest absolute intensities | 8 |
| Figure S8. Isotopic fine structure acquired directly from a root nodule using LAESI-MS | 9 |

Supporting Figures

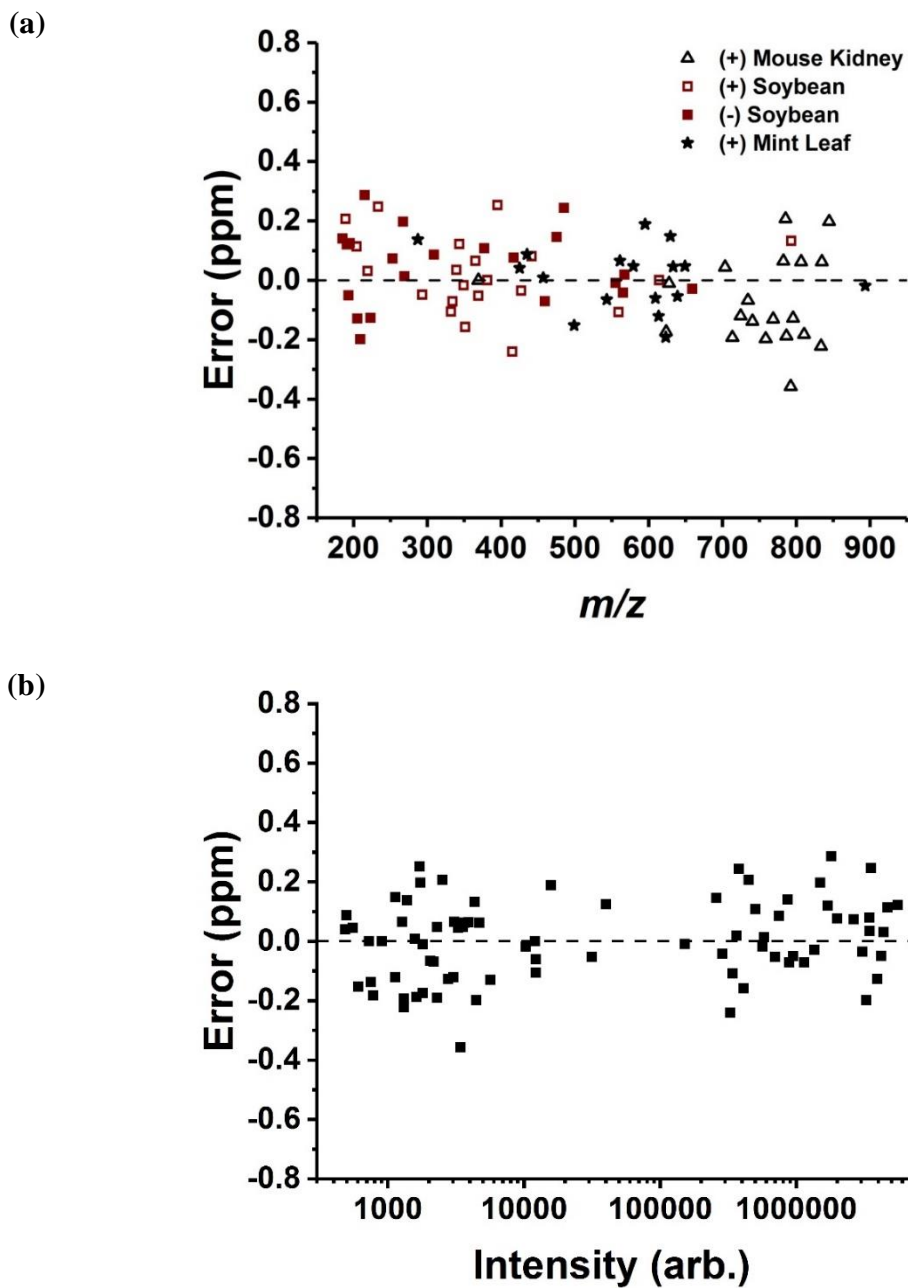


Figure S1. Mass measurement errors as a function of (a) m/z and (b) peak intensities for the annotated compounds in Tables S1-S4 acquired by LAESI-21T-FTICR-MS analysis of soybean root nodules, mouse kidney sections, and whole mint leaves. Cutoff for mass measurement error was 0.4 ppm for all annotations and elemental compositions.

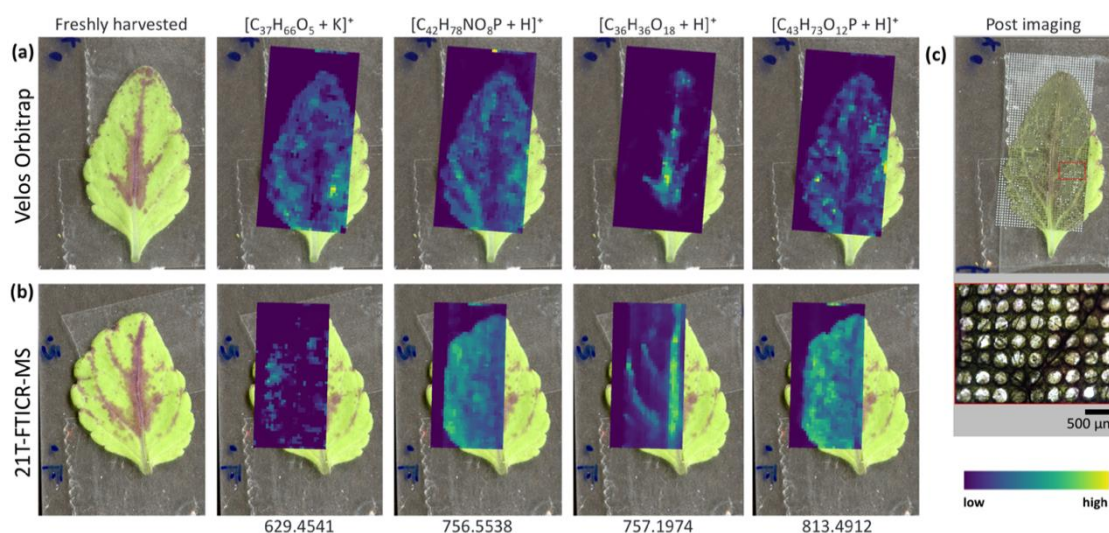


Figure S2. Comparison of LAESI-MS images with source coupled to (a) LTQ Orbitrap Velos and (b) 21T-FTICR. Freshly harvested common coleus leaves were analyzed without sample preparation, and (c) imaged using a stage with step size of 300 μm and laser focal spot size of ~ 200 μm . Spatial distributions of $[\text{C}_{37}\text{H}_{66}\text{O}_5 + \text{K}]^+$ (m/z 629.4541), $[\text{C}_{42}\text{H}_{78}\text{NO}_8\text{P} + \text{H}]^+$ (m/z 756.5538), $[\text{C}_{36}\text{H}_{36}\text{O}_{18} + \text{H}]^+$ (m/z 757.1974), and $[\text{C}_{43}\text{H}_{73}\text{O}_{12}\text{P} + \text{H}]^+$ (m/z 813.4912) are presented as examples of molecular imaging by a LAESI source coupled to FTMS systems. Putative molecular identifications for these species are DG(32:3), PC(34:3), a number of possible flavonoid c-glycosides, and PI(34:6), and their structural isomers, respectively. Molecular formula annotations and putative identifications were generated from METASPACE. Specifically, the molecular annotation for m/z 629.4541, 756.5538, and 813.4912 were made using the SwissLipids database, and the molecular annotation for m/z 757.1974 was made from the HMDB v2.5-Cotton database. Underlying data can be found at

http://metaspaces2020.eu/#/annotations?db=SwissLipids-2018-02-02&ds=2018-05-14_17h08m35s&fdr=0.2 for LTQ Orbitrap Velos, and

http://metaspaces2020.eu/#/annotations?db=SwissLipids-2018-02-02&ds=2018-05-14_17h00m13s&fdr=0.2 for 21T-FTICR-MS.

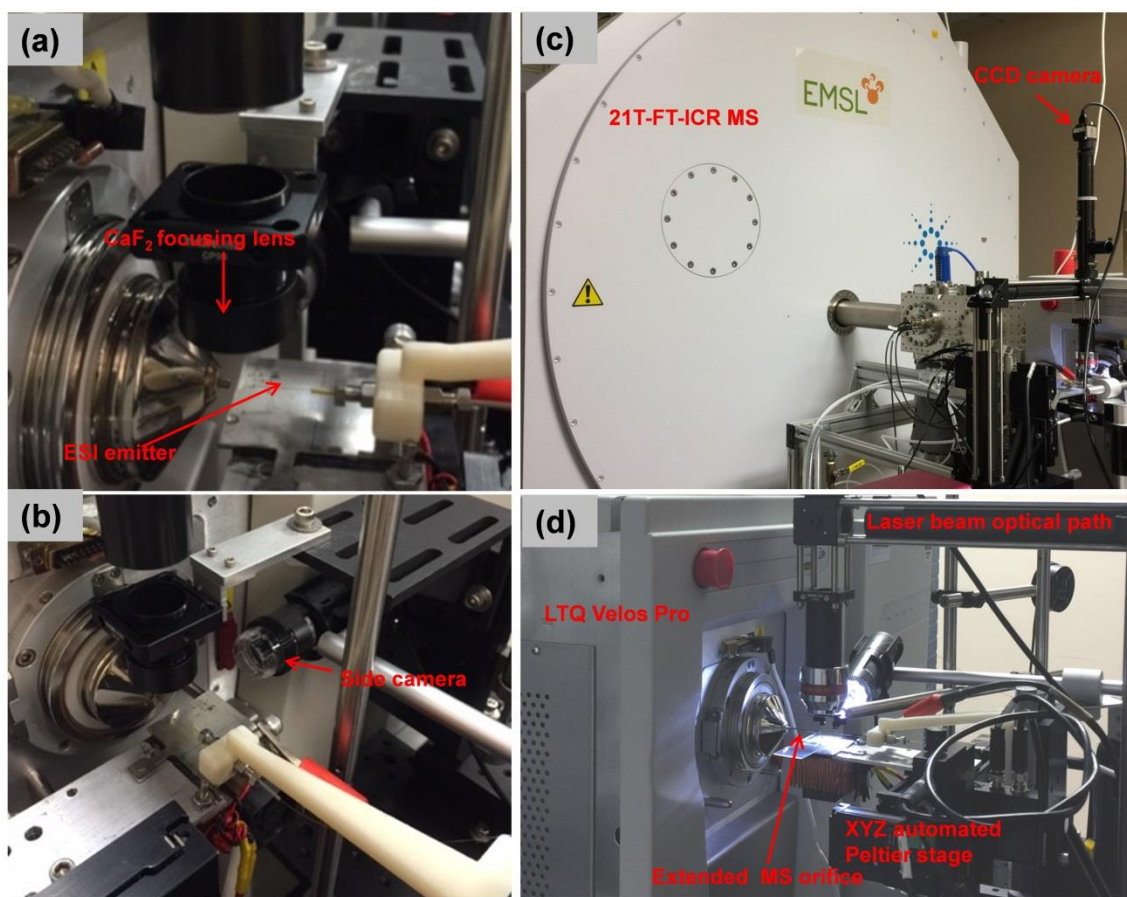


Figure S3. (a-b) Images of homebuilt LAESI source coupled to an LTQ Orbitrap Velos system used for source development. (c-d) Images of LAESI source coupled to a 21T-FTICR-MS housed at EMSL (see diagram in Figure 1).

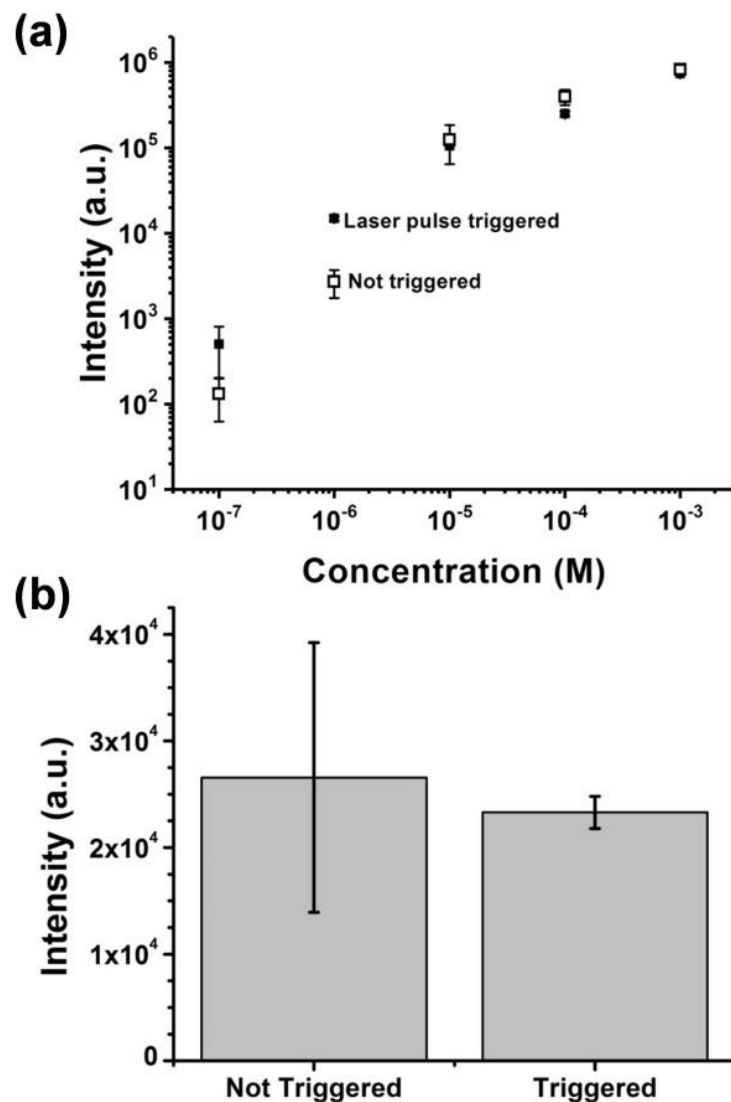


Figure S4. (a) LAESI-MS peak intensities for verapamil solutions of different concentrations, where laser pulses were synchronized (triggered) or not synchronized (not triggered) with ion trap filling. (b) Intensity variability ($n = 10$) for positive ions from $1 \mu\text{M}$ verapamil solution in triggered and non-triggered modes. Laser operated at 20 Hz repetition rate (4.5 ± 0.2 mJ pulse energy) with 200 ms injection times (ion trap fill time) on LTQ Orbitrap Velos instrument.

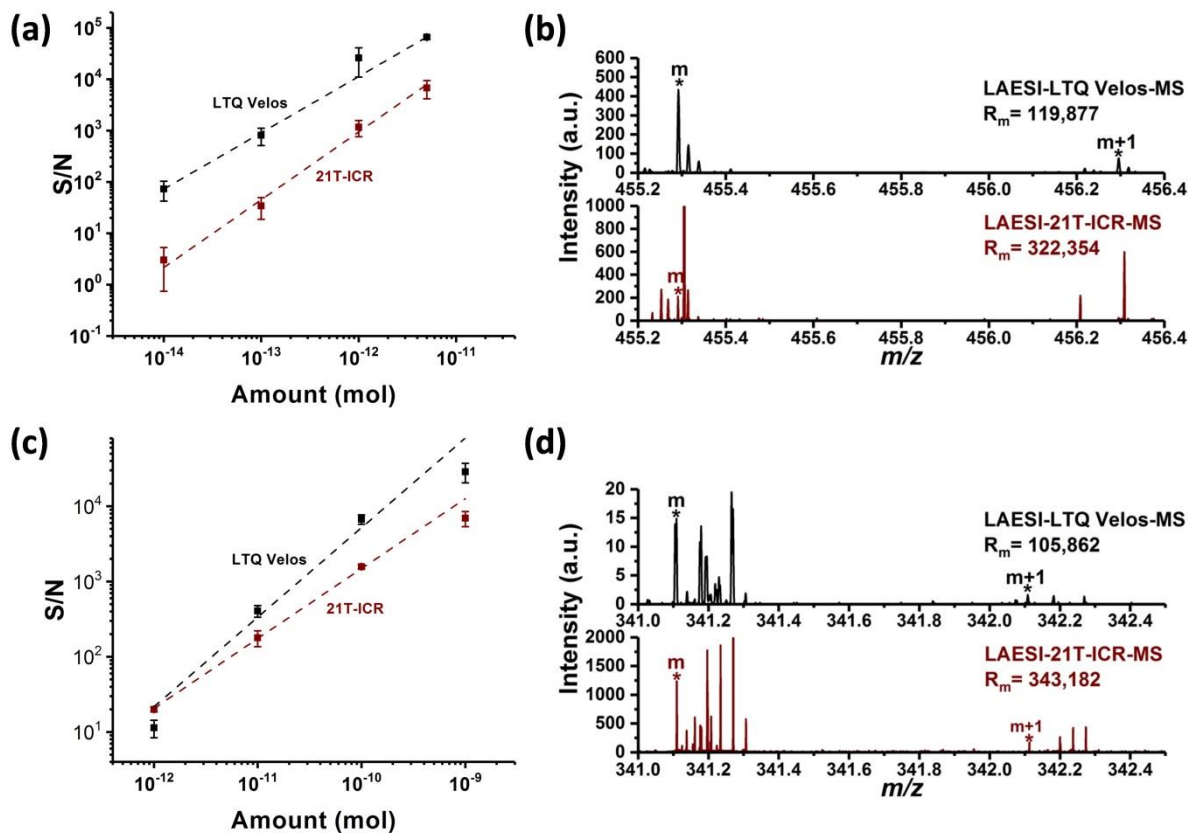


Figure S5. Sensitivities for LAESI-MS with LTQ Orbitrap Velos and 21T-FTICR mass spectrometers using $TT = 0.768$ s, laser pulse energy of 1.5 ± 0.2 mJ, and 200 ms injection times (four laser shots per fill). (a) Positive ion mode limit of detection curve for verapamil with (b) corresponding mass spectra for a 10-fmol sample using LTQ Orbitrap Velos-MS and 21T-FTICR-MS. (c) In negative ion mode, sucrose was used to evaluate the sensitivities of the two platforms. (d) Corresponding mass spectra for 1 pmol sample. Signal intensity is represented by the signal-to-noise ratio, where noise was measured in each spectrum.

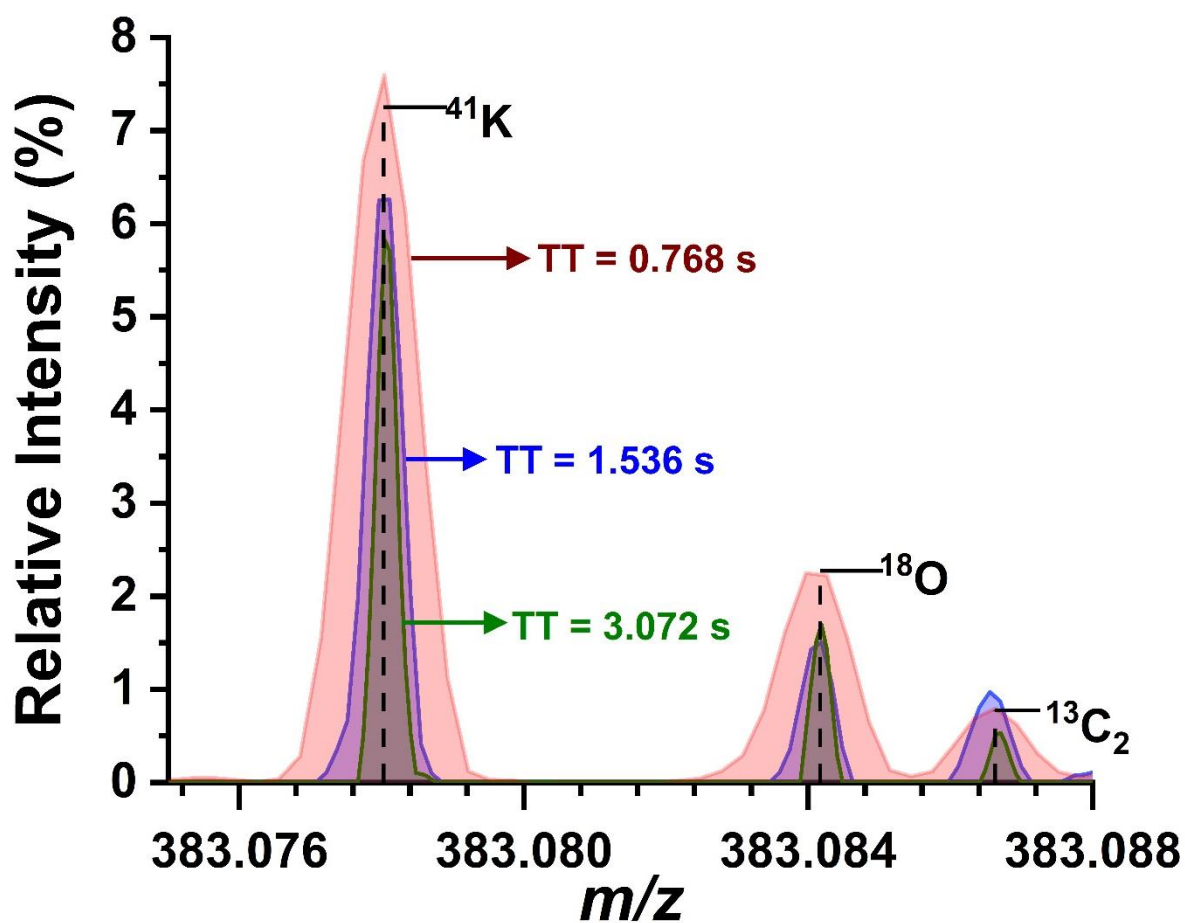


Figure S6. Comparison of LAESI mass spectra for soybean root nodule at three different TT values (TT = 0.768 s, 1.536 s, and 3.072 s) in the mass range that contains the $M+2$ isotopologues of a disaccharide peak (i.e., $[\text{M}+\text{K}]^+$). Dotted vertical lines refer to the theoretical centroids and amplitudes for ^{41}K , ^{18}O , and $^{13}\text{C}_2$ natural isotopes.

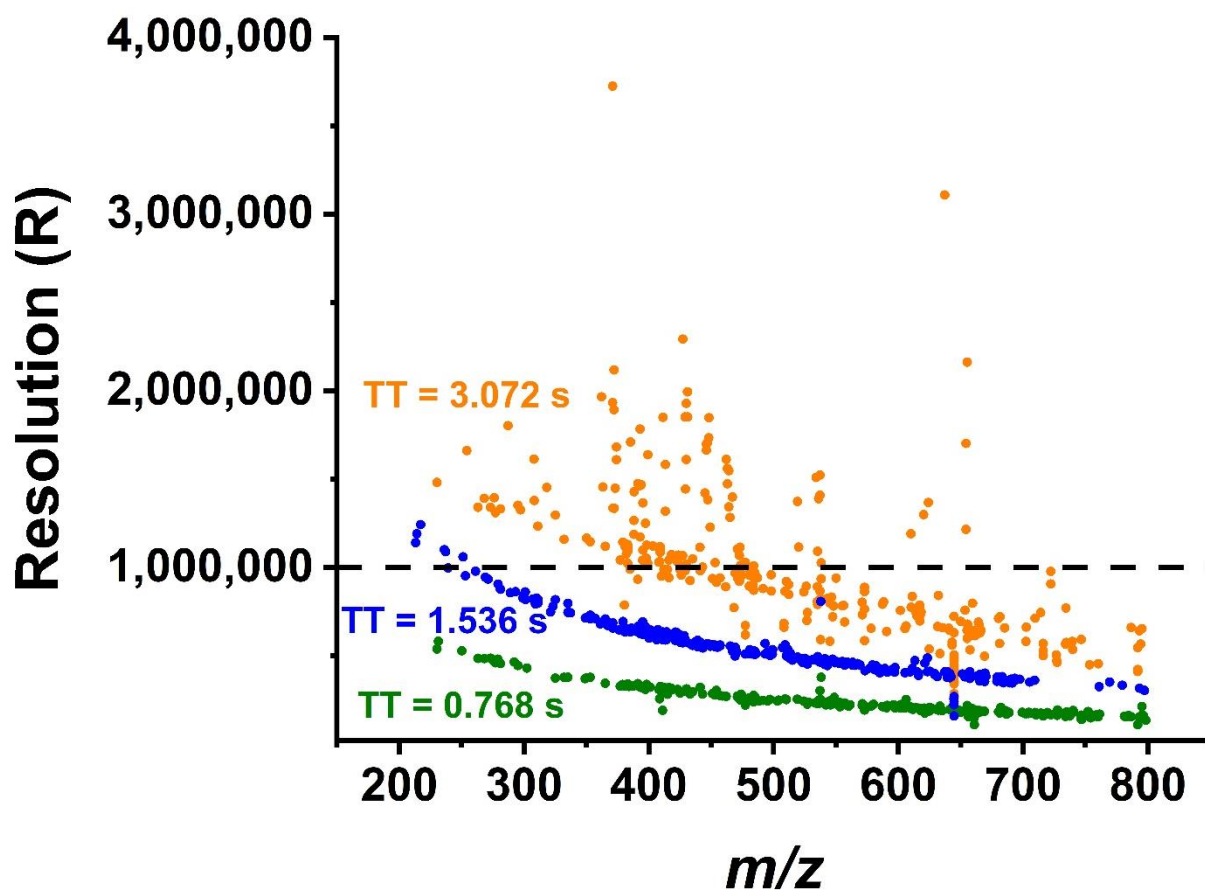


Figure S7. Resolving power for 300 peaks with highest absolute intensities from representative soybean root nodule spectra at TT = 0.768 s, 1.536 s, and 3.072 s. At TT = 3.072 s, peaks in lower mass range ($m/z < 450$) showed $R > 1,000,000$. At shortest TT of 0.768 s a maximum resolution of 500,000 was observed for $m/z < 350$.

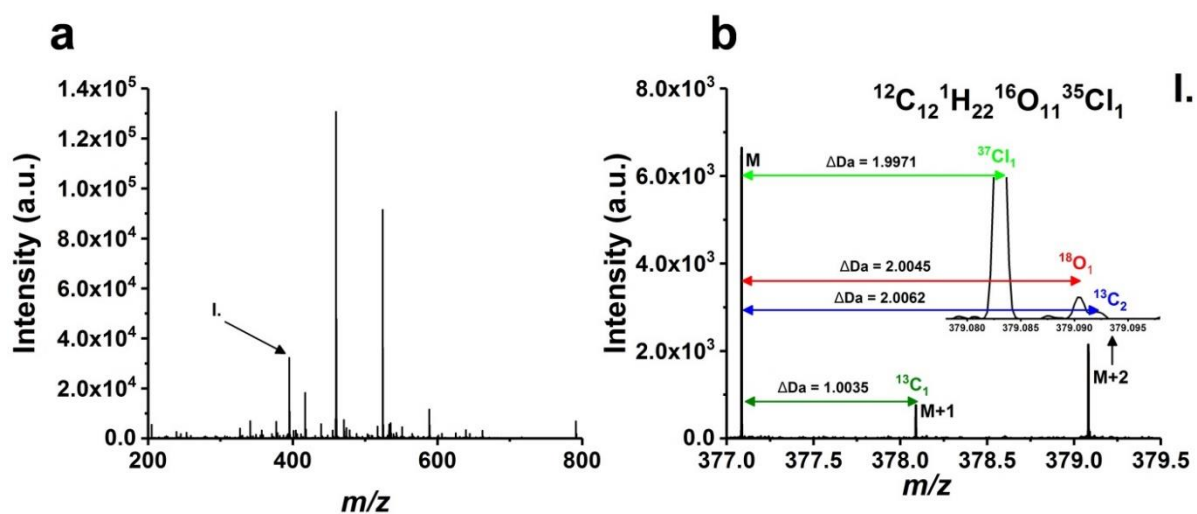


Figure S8. (a) Isotopic fine structure acquired directly from a root nodule using LAESI-MS. Feature at m/z 377.0859 labeled as (I) was tentatively annotated as $\text{C}_{12}\text{H}_{22}\text{O}_{11}\text{Cl}_1$, which corresponds to hexose with a Cl adduct. (b) Zoomed spectrum with M, M+1, and M+2 peaks showed IFS with isotopologues containing $^{37}\text{Cl}_1$, $^{18}\text{O}_1$, $^{13}\text{C}_1$, and $^{13}\text{C}_2$.